RESEARCH ARTICLE

Structural and Electrical Properties of $Sr_2Fe_{0.75}Co_{0.75}Mn_{0.5}O_{6-\delta}$.

Ram Krishna Hona[1], Amara Martinson[1], Alexa D. Azure[2], Mandy Guinn[1]

[1]*Environmental Science Department, United Tribes Technical College, Bismarck, ND 58504, USA.*
[2]*Engineering Department, United Tribes Technical College, Bismarck, ND 58504, USA.*

Abstract

This study introduces a novel oxygen-deficient perovskite, $Sr_2Fe_{0.75}Co_{0.75}Mn_{0.5}O_{6-\delta}$, synthesized through a solid-state reaction and thoroughly characterized by Powder XRD, SEM and direct current (DC) electrical conductivity measurements. The material, exhibiting a cubic crystal structure with the $Pm\overline{3}m$ space group, demonstrates intriguing electrical properties. At temperatures ranging from 25 to 400 °C, the material displays semiconductor-type conductivity, transitioning seamlessly to metallic-type conductivity from 400 to 800 °C. The deliberate incorporation of cobalt into the perovskite structure is found to be pivotal, as evidenced by a comparative analysis with its parent compound, $Sr_2FeMnO_{6-\delta}$. This investigation reveals a substantial improvement in electrical conductivity, underscoring the significance of the partial substitution of cobalt. The tailored electrical properties of $Sr_2Fe_{0.75}Co_{0.75}Mn_{0.5}O_{6-\delta}$ position it as a versatile candidate for electronic applications.

1. Introduction

Perovskite oxides (POs) are applicable to high-temperature oxygen separation, membrane reactors, solid oxide fuel cells[1], as semiconductors for thermoelectric devices[2] and solar cells[3], and as electrocatalysts for oxygen evolution reactions[4, 5]. Since all these applications are related to material properties such as the charge transport properties, it is crucial to characterize such materials and study the electrical properties of POs.

POs are simply perovskites with general formula ABO_3 or $A_2B_2O_6$ where A, B and δ represent alkaline earth metals or lanthanides, transition metals and they can be represented as $ABO_{3-\delta}$ or $A_2B_2O_{6-\delta}$ when they have some oxygen deficiency. Here, δ represents the amount of oxygen deficiency. When substitutions are made in the A or B cations, it often leads to structural

or phase transformations, influencing the material properties.[6] For instance, different B-site cations can result in variations in structure and properties. For example, the nature of the B-site cation affects the structure and properties. $Ca_2Mn_2O_5$[7] and $Ca_2Cr_2O_5$[8] are oxygen deficient perovskites and have defect-ordered structures, but the type of ordering in these two compounds is different. $Ca_2Mn_2O_5$ contains only one type of B-site coordination, namely square pyramidal MnO5 units. However, $Ca_2Cr_2O_5$ contains alternating layers of CrO4 tetrahedra and CrO6 octahedra, forming the so-called brownmillerite-type structure. These structural differences result in very different magnetic and electrical properties. Similarly, $Sr_2Fe_2O_{6-\delta}$ has a tetrahedral structure with FeO_5 square pyramidal dimers while one Fe is substituted by Co to get $Sr_2FeCoO_{6-\delta}$, the crystal transforms to cubic structure.[6, 9] In some cases, even small variation, ~5%,

of the B-site cation can cause significant changes to the distribution of defects in the structure, as observed for $Sr_2Fe_{1.9}Cr_{0.1}O_{6-\delta}$ (cubic *Pm-3m*) and $Sr_2Fe_{1.9}Co_{0.1}O_{6-\delta}$ (orthorhombic *Cmmm*) as compared to its parent compound $Sr_2Fe_2O_{6-\delta}$ (tetrahedral).[9, 10] Most of the structural or phase transformation studies involve materials with only one or two types of elements at B site. There are very few studies for other class of materials with more than two different elements at B site. Some of the materials containing three different elements at the B site are $LiNiMnCoO_2$ (NMC) and $LiNi_{0.8}Co_{0.15}Al_{0.05}O_2$ (NCA) which is derived from $LiCoO_2$ (LCO) and $LiMnO_2$ (LMO) by substituting B site element.[11, 12] All these four compounds are used as battery materials. Researchers have reported the advantages of these three element-containing materials, NMC and NCA over the parent materials. It means material properties can be improved by introducing more than two different elements at the B site. However, as we discussed before, structural or phase changes are more likely with the introduction of different elements at the B site.

In this work, we report the introduction of a fraction of Co to $Sr_2FeMnO_{6-\delta}$ to get $Sr_2Fe_{0.75}Co_{0.75}Mn_{0.5}O_{6-\delta}$ that consists of three different elements at the B site. This new composition retains the cubic structure with $Pm\overline{3}m$ space group. This work also provides the information of significant improvement of the conductivity after Co incorporation.

This research highlights the structural and phase stability of oxygen-deficient perovskites with three different elements at the B site. The introduction of Co brings about improved conductivity, showcasing the potential for tailoring material properties in complex perovskite structures for various applications.

2. Experiment

The $Sr_2Fe_{0.75}Co_{0.75}Mn_{0.5}O_{6-\delta}$ sample was synthesized using the conventional solid-state synthesis method.

Initially, powders of precursor compounds, namely $SrCO_3$, Mn_2O_3 and Fe_2O_3 were mixed and ground using an agate mortar and pestle. The resulting mixture was then pressed into a pellet and subjected to heating at 1000 °C for 24 hours in an air environment.

Subsequently, the samples underwent regrinding and were re-fired at 1200 °C for 24 hours in the same conditions, followed by a slow cooling process. The heating and cooling rates during both firings were maintained at 100 °C/h. The phase purity and structure of the polycrystalline samples were characterized by powder X-ray diffraction (XRD) at room temperature, employing a Bruker D2 phaser diffractometer with Cu Kα1 (λ = 1.54056 Å). Rietveld refinements were conducted using GSAS software and the EXPEGUI interface.

The microstructures of the samples were examined through scanning electron microscopy (SEM). The electrical properties of the samples were assessed through direct-current (dc) measurements on pellets sintered at 1200 °C. The 2-probe dc measurements were conducted in the temperature range of 25-800 ºC, applying a constant voltage of 10 mV and collecting the output current. The rate of heating for conductivity measurements was set at 5 °C/min.

3. Results and Discussion

3.1 Crystal Structure

The crystal structures of the compounds were assessed by Powder XRD, and their Rietveld refinement analysis revealed that both $Sr_2FeMnO_{6-\delta}$ and $Sr_2Fe_{0.75}Co_{0.75}Mn_{0.5}O_{6-\delta}$ exhibit a cubic structure with the space group $Pm\overline{3}m$. $Sr_2FeMnO_{6-\delta}$ has been previously reported.[13] Figure 1 displays the Rietveld refinement profile and crystal structure of the material, $Sr_2Fe_{0.75}Co_{0.75}Mn_{0.5}O_{6-\delta}$. In these structures of ODPs, vacancies are distributed randomly, yet the octahedra share corners, reminiscent of simple cubic perovskite structures.
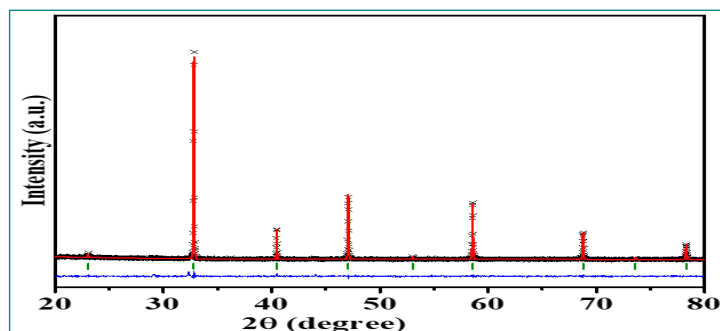

Figure 1. *Rietveld refinement profile for powder XRD data of $Sr_2Fe_{0.75}Co_{0.75}Mn_{0.5}O_{6-\delta}$ refined in the space group $Pm\overline{3}m$. Crosses represent experimental data, the solid red line is the model, vertical green tick marks show Bragg peak positions, and the lower blue line represents the difference plot.*

The refined structural parameters for $Sr_2Fe_{0.75}Co_{0.75}Mn_{0.5}O_{6-\delta}$ can be found in Table 1. As depicted in the figure 1, the BO6 octahedra share corners with other octahedra, where B represents the central atom in the octahedron, and oxygens lie at the corners of the octahedron. Four of these octahedra surround the Sr cation, seemingly 12-coordinated with corner-shared oxygens (refer to Figure 1). For comparison, the parent compound $Sr_2FeMnO_{6-\delta}$ has also been studied. It was found cubic with $Pm\overline{3}m$ space group as in previous report.[13] Table 2 shows the refined structural parameters of $Sr_2FeMnO_{6-\delta}$. The incorporation of Co does not change the structural dimensions (length and volume).

Table 1. *Refined structural parameters for $Sr_2Fe_{0.75}Co_{0.75}Mn_{0.5}O_{6-\delta}$ using powder X-ray diffraction data.*

Space group: *$Pm\overline{3}m$, a = 3.8585(2)Å, V = 57.445(3) Å3, Rp=0.0459, wRp= 0.0605 $\chi2$ = 1.40*

Elements	x	y	z	Uiso	Occupancy	Multiplicity
Sr1	0.00	0.00	0.00	0.0237(2)	1	1
Fe1	0.50	0.50	0.50	0.0298(5)	0.375	1
Mn1	0.50	0.50	0.50	0.0298(5)	0.25	1
Co1	0.50	0.50	0.50	0.0298(5)	0.375	1
O1	0.00	0.50	0.50	0.0227(1)	0.99	3

Table 2. *Refined structural parameters for $Sr_2FeMnO_{6-\delta}$ using powder X-ray diffraction data*

Space group: *Pm-3m, a = 3.8504(5)Å, V = 57.084(4)Å3, Rp=0.0300, wRp= 0.0387, $\chi2$ = 1.02*

Elements	x	y	z	Uiso	Occupancy	Multiplicity
Sr1	0.0	0.0	0.0	0.0230(6)	1	1
Fe1	0.5	0.5	0.5	0.0251(8)	0.5	1
Mn1	0.5	0.5	0.5	0.0711(8)	0.5	1
O1	0.0	0.5	0.5	0.0431(1)	0.963	3

To delve into the microstructure of $Sr_2Fe_{0.75}Co_{0.75}Mn_{0.5}O_{6-\delta}$, scanning electron microscopy (SEM) was employed. Figure 2 showcases SEM images of the as-prepared pellets of the material. It is apparent that the grain growth is irregular, accompanied by the presence of pores."
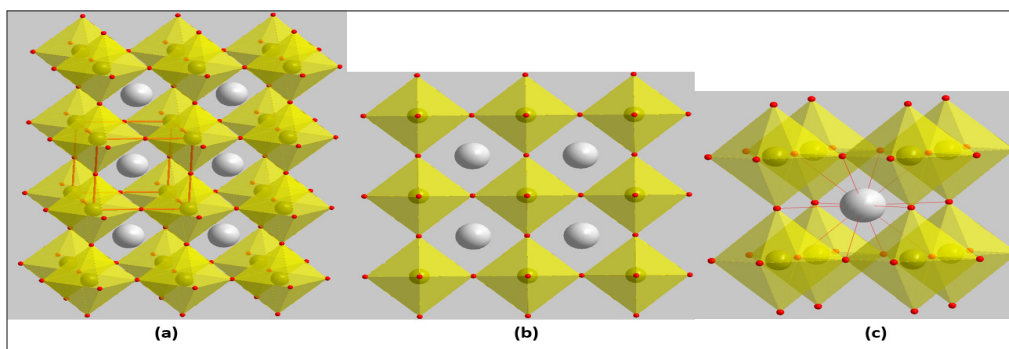

Figure 2. *crystal structure of $Sr_2Fe_{0.75}Co_{0.75}Mn_{0.5}O_{6-\delta}$ (a) Crystallographic unit cell and corner-sharing (Fe/Co/Mn)O6 octahedra (yellow) are highlighted. The large white-gray spheres are the Sr atoms. (b) View along the unit cell axis. Because of the cubic symmetry, the three axes are identical. (c) Coordination geometry around the Sr atom, which is 12-coordinated.*
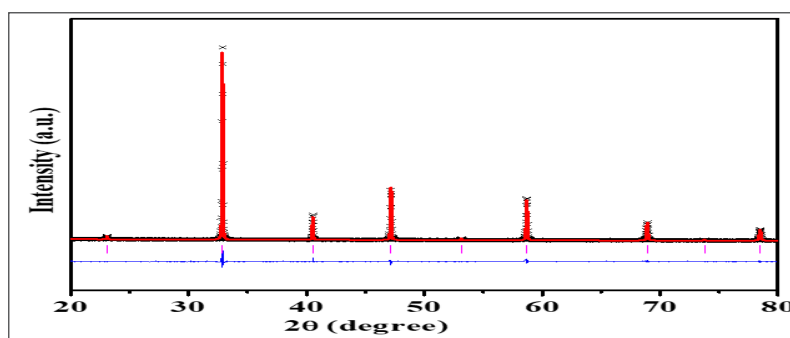

Figure 3. *Rietveld refinement profile for powder XRD data of $Sr_2FeMnO_{6-\delta}$ refined in the space group $Pm\overline{3}m$. Crosses represent experimental data, the solid red line is the model, vertical pink tick marks show Bragg peak positions, and the lower blue line represents the difference plot.*
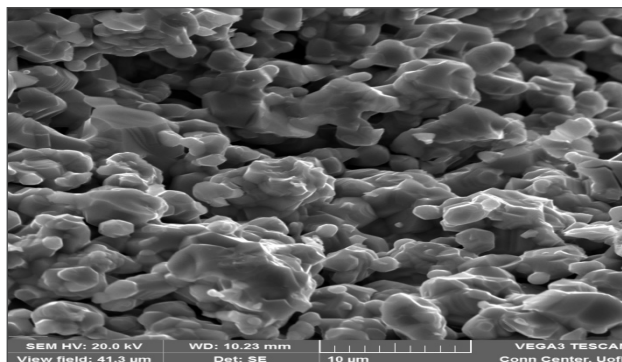
Figure 4. *SEM image of $Sr_2Fe_{0.75}Co_{0.75}Mn_{0.5}O_{6-\delta}$.*

3.2 Electrical Properties

The charge transport characteristics of the materials were investigated using the 2-probe DC measurement method. This technique involves maintaining a constant applied current or voltage to measure the corresponding output voltage or current. The total conductivity (σ) was calculated using the relationship σ = L/RA, where L, R, and A denote the thickness, resistance, and cross-sectional area of the cylindrical/disc pellet, respectively. Table 2 presents the total conductivity values for these materials at room temperature.

Introducing Co as a dopant in $Sr_2FeMnO_{6-\delta}$, resulting in the composition $Sr_2Fe_{0.75}Co_{0.75}Mn_{0.5}O_{6-\delta}$, led to a three-order of magnitude improvement in room temperature conductivity. Figure 5 illustrates the conductivity data for both materials, indicating that $Sr_2Fe_{0.75}Co_{0.75}Mn_{0.5}O_{6-\delta}$ behaves as a semiconductor up to 400 °C. Beyond this temperature, there is a downturn in conductivity, decreasing with temperature up to 800 °C. In contrast, the conductivity of $Sr_2FeMnO_{6-\delta}$ increases steadily with temperature, exhibiting no downturn up to 800 °C, though it exhibits sigmoidal type conductivity shape as shown in figure 5 inset.
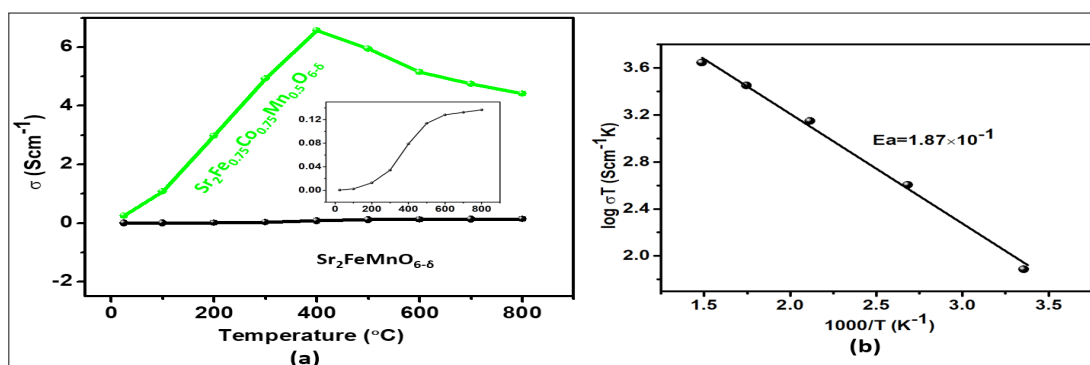

Figure 5. *a) Total conductivity of $Sr_2Fe_{0.75}Co_{0.75}Mn_{0.5}O_{6-\delta}$ (green) and $Sr_2FeMnO_{6-\delta}$ (black) as a function of temperature. The inset represents the enlargement of $Sr_2FeMnO_{6-\delta}$ (black). b) Activation energy of $Sr_2Fe_{0.75}Co_{0.75}Mn_{0.5}O_{6-\delta}$ obtained at 25-400 °C using Arrhenius equation.*

The electrical conductivity in oxygen-deficient perovskites relies on electron hopping through a metal–oxygen–metal (M–O–M) bond system.[14, 15] Metals with multiple oxidation states ($M^{2+}/M^{3+}/M^{4+}$) on the B-site facilitate this process. In our materials, M-3d orbitals overlap with oxygen 2p orbitals, enabling electron hopping through the $M^{2+/3+}–O^{2-}–M^{3+/4+}$ pathway.[15] To comprehend the temperature-dependent conductivity, variable-temperature studies were conducted, revealing a similar conductivity trend observed in other ODPs.

As temperature rises, charge carrier mobility increases, leading to enhanced electrical conductivity. This temperature-activated mobility is described by the relationship σ = neμ, where σ is conductivity, n is the concentration of electrons/holes, e is the charge of the electron, and μ is the mobility of the charge carriers.[16] P-type semi conductivity is characteristic of semiconducting ODPs, where electron holes are the primary charge carriers.[15-17]

There is a limit to the temperature-activated increase in polaron mobility, beyond which collisions between phonons and charge carriers result in decreased conductivity, resembling a metal-like temperature-dependent behavior.[18] Some researchers attribute this conductivity decrease to the loss of oxygen and disruption of $M3^{+}–O^{2-}–M^{4+}$ conduction pathways.[19,20]

The energy of activation for temperature-dependent conductivity was determined using the Arrhenius equation, $\sigma T = \sigma° e^{(-Ea/KT)}$.[16, 21] Figure 5 displays the Arrhenius plot for conductivity in the temperature range of 25-800 °C. The slope of the plot changes at high temperatures, consistent with the change in conductivity trend. This leads to two different E_a values, with the activation energy at high temperature being negative. Table 3 shows the E_a value for 25-400 °C of $Sr_2Fe_{0.75}Co_{0.75}Mn_{0.5}O_{6-\delta}$. The E_a value above 400 °C is not reported because of the negative value. Similarly, the E_a value of $Sr_2FeMnO_{6-\delta}$ is also not shown because of the sigmoidal conductivity.

Table 3. *Total Conductivity, σ (S cm−1) and activation energies, Ea (eV).*

Compounds	25 ºC	800 ºC	[Ea (eV)]
$Sr_2FeMnO_{6-\delta}$	5.4195×10^{-4}	1.366×10^{-1}	N/A
$Sr_2Fe_{0.75}Co_{0.75}Mn_{0.5}O_{6-\delta}$	2.583×10^{-1}	4.415×10^{0}	1.87×10^{-1} (25-400 ºC)

4. Conclusion

A new perovskite oxide, $Sr_2Fe_{0.75}Co_{0.75}Mn_{0.5}O_{6-\delta}$, has been synthesized using a solid-state reaction method. The XRD analysis revealed that the material has a cubic crystal structure with a *pm-3m* phase. The electrical charge transport properties of $Sr_2Fe_{0.75}Co_{0.75}Mn_{0.5}O_{6-\delta}$ were investigated at different temperatures. The results indicate that the material exhibits semiconductor-type conductivity in the temperature range of 25 to 400 °C and metallic-type conductivity from 400 to 800 °C. This means that the electrical behavior of the material changes from that of a semiconductor to that of a metal as the temperature increases within these specified ranges.

Furthermore, we compared the electrical conductivity of $Sr_2Fe_{0.75}Co_{0.75}Mn_{0.5}O_{6-\delta}$ with another material, $Sr_2FeMnO_{6-\delta}$, to highlight the improvement in conductivity achieved by partially substituting Fe and Mn with Co in the new material. This suggests that the introduction of cobalt has a positive impact on the electrical conductivity of the perovskite oxide, making it a potentially interesting material for various applications, particularly those requiring tunable electrical properties.

Institutional Review Board Statement: Not Applicable

Informed Consent Statement: Not applicable

Conflicts of Interest: The authors declare no conflict of interest.

5. References

1. Sunarso, J.; Hashim, S. S.; Zhu, N.; Zhou, W., Perovskite oxides applications in high temperature oxygen separation, solid oxide fuel cell and membrane reactor: A review. *Prog. Energy Combust. Sci.* 2017, *61*, 57-77.

2. Wu, T.; Gao, P., Development of Perovskite-Type Materials for Thermoelectric Application. *Materials* 2018, *11* (6).

3. Bera, A.; Wu, K.; Sheikh, A.; Alarousu, E.; Mohammed, O. F.; Wu, T., Perovskite Oxide SrTiO3 as an Efficient Electron Transporter for Hybrid Perovskite Solar Cells. *J. Phys. Chem. C 2014, 118* (49), 28494-28501.

4. Hona, R. K.; Ramezanipour, F., Remarkable Oxygen-Evolution Activity of a Perovskite Oxide from the Ca2−xSrxFe2O6−δ Series. *2019*, *58* (7), 2060-2063.

5. Hona, R. K.; Karki, S. B.; Cao, T.; Mishra, R.; Sterbinsky, G. E.; Ramezanipour, F., Sustainable Oxide Electrocatalyst for Hydrogen- and Oxygen-Evolution Reactions. *ACS Catalysis 2021, 11* (23), 14605-14614.

6. Hona, R. K.; Huq, A.; Ramezanipour, F., Unraveling the Role of Structural Order in the Transformation of Electrical Conductivity in Ca2FeCoO6−δ, CaSrFeCoO6−δ, and Sr2FeCoO6−δ. *Inorg. Chem. 2017*, *56* (23), 14494-14505.

7. Kim, J.; Yin, X.; Tsao, K.-C.; Fang, S.; Yang, H., Ca2Mn2O5 as Oxygen-Deficient Perovskite

Electrocatalyst for Oxygen Evolution Reaction. *J. Am. Chem. Soc.* 2014, *136* (42), 14646-14649.

8. Arevalo-Lopez, A. M.; Attfield, J. P., Crystal and magnetic structures of the brownmillerite Ca2Cr2O5. *Dalton Trans. 2015, 44* (23), 10661-10664.

9. Hona, R. K.; Huq, A.; Mulmi, S.; Ramezanipour, F., Transformation of Structure, Electrical Conductivity, and Magnetism in AA'Fe2O6−δ, A = Sr, Ca and A' = Sr. *Inorg. Chem. 2017*, *56* (16), 9716-9724.

10. Ramezanipour, F.; Greedan, J. E.; Cranswick, L. M. D.; Garlea, V. O.; Siewenie, J.; King, G.; Llobet, A.; Donaberger, R. L., The effect of the B-site cation and oxygen stoichiometry on the local and average crystal and magnetic structures of Sr2Fe1.9M0.1O5+y (M = Mn, Cr, Co; y = 0, 0.5). *J. Mater.Chem. 2012*, *22* (19), 9522-9538.

11. Choi, J.-W.; Kim, J.; Kim, S.-K.; Yun, Y.-S., Simple, green organic acid-based hydrometallurgy for waste-to-energy storage devices: Recovery of NiMnCoC2O4 as an electrode material for pseudocapacitor from spent LiNiMnCoO2 batteries. *J.Hazard. Mater. 2022*, *424*, 127481.

12. Cai, C.; Hensley, D.; Koenig, G. M., High capacity rechargeable coin cells using all active material electrodes and percolated networks of LiCoO2 blended with LiNi0.8Co0.15Al0.05O2. *J. Alloys and Compd. 2023*, *968*, 171965.

13. Mulmi, S.; Hona, R. K.; Jasinski, J. B.; Ramezanipour, F., Electrical conductivity of Sr2-xCaxFeMnO5 (x = 0, 1, 2). *J. Solid State Electrochem. 2018, 22* (8), 2329-2338.

14. Mineshige, A.; Inaba, M.; Yao, T.; Ogumi, Z.; Kikuchi, K.; Kawase, M., Crystal Structure and Metal–Insulator Transition of La1−xSrxCoO3. *J. Solid State Chem. 1 1996, 121* (2), 423-429.

15. Asenath-Smith, E.; Misture, S. T.; Edwards, D. D., Structural behavior and thermoelectric properties of the brownmillerite system Ca2(ZnxFe2−x)O5. *J. Solid State Chem. 2011, 184* (8), 2167-2177.

16. Asenath-Smith, E.; Lokuhewa, I. N.; Misture, S. T.; Edwards, D. D., p-Type thermoelectric properties of the oxygen-deficient perovskite Ca2Fe2O5 in the brownmillerite structure. *J. Solid State Chem. 2010, 183* (7), 1670-1677.

17. Ren, P.; Masó, N.; Liu, Y.; Ma, L.; Fan, H.; West, A. R., Mixed oxide ion and proton conduction and p-type semiconduction in BaTi0.98Ca0.02O2.98 ceramics. *J. Mater.Chem. C 2013*, *1* (13), 2426-2432.

18. Yu, H.-C.; Fung, K.-Z., Role of Sr Addition on the Structure Stability and Electrical Conductivity of Sr-Doped Lanthanum Copper Oxide Perovskites. *J. Mater. Res. 2004, 19* (3), 943-949.

19. Armstrong, T.; Prado, F.; Manthiram, A., Synthesis, crystal chemistry, and oxygen permeation properties of LaSr3Fe3−xCoxO10 (0≤x≤1.5). *Solid State Ionics 2001, 140* (1), 89-96.

20. Chen, Z.; Ran, R.; Zhou, W.; Shao, Z.; Liu, S., Assessment of Ba0.5Sr0.5Co1−yFeyO3−δ (y=0.0–1.0) for prospective application as cathode for IT-SOFCs or oxygen permeating membrane. *Electrochim. Acta 2007*, *52* (25), 7343-7351.

21. Andoulsi, R.; Horchani-Naifer, K.; Férid, M., Electrical conductivity of La1−xCaxFeO3−δ solid solutions. *Ceram.Int. 2013*, *39* (6), 6527-6531.